ROYAL
AERONAUTICAL
SOCIETY

REGULAR PAPER

Investigation on frequency influence on the transverse pulsed jet in a supersonic crossflow

Z.-Z. Xu , Y.-M. Zhou , J.-P. Wu* and W. Huang* [ID]

College of Aerospace Science and Engineering, National University of Defense Technology, Changsha, Hunan 410073, People's Republic of China
*Correspondence authors. Emails: wujiping07@nudt.edu.cn, gladrain2001@163.com

Abstract

The pulsed jet is a novel and effective active mixing enhancement approach. For the transverse pulsed jet in the supersonic crossflow, the frequency influence is investigated using the three-dimensional Reynolds-averaged Navier–Stokes (RANS) equations coupled with the SST k-ω turbulence model. The averaged flow field properties of the pulsed jet are better than those of the steady jet when considering mixing efficiency and jet penetration depth, especially for the case with the pulsed frequency being 50kHz. The flow field structures of the pulsed jet are connected with the time, with periodic wave structures generating in the flow field and moving downstream. The size of the wave structures and its distance are related to the frequency, namely the size and flow distance are relatively small at 50kHz, and it takes some time for the pulsed jet to establish its influence in the full flow field. At low frequencies, the flow field produces large fluctuations, and this may be detrimental to the stable operation of the engine.

Nomenclature

AUSM	advection upstream splitting method
RANS	reynolds-averaged navier stokes
Scramjet	supersonic combustion ramjet engine
SST	shear stress transfer
UDF	user-defined function
A	axial area of mixing, mm^2
D	diameter of the injector, mm
f_i	frequency of the pulsed jet, $i = 1, 2$ and 3, kHz
J	momentum flux ratio
J_0	benchmark momentum flux ratio
J_a	amplitude of sinusoidal variation
P_{H2}	penetration depth, mm
t	flow time, s
u	local velocity, m/s
x, y, z	Coordinates, mm
α	mass fraction of fuel
α_{stoic}	mass fraction of fuel at the chemical equivalence ratio
ρ	local density, kg/m^3
η_{mix}	mixing efficiency

1.0 Introduction

The scramjet engine has a broad application prospect, and one of the key working processes in the engine is fuel mixing and combustion. At present, the fuel supply mode is generally strut and wall injection. After entering the combustor, the fuel is in the environment of supersonic flow, so it is difficult to mix, ignite and stable combust. In order to improve the engine performance, it is necessary to improve the fuel mixing and combustion efficiencies so that the engine can obtain effective thrust, and the key is the mixing enhancement technology. In the past, the researchers considered the flow field characteristics and mixing effect of the jet from the aspects of the injector configuration [1], the number of injectors [2], the fuel injection angle [3] and the fuel type [4]. Huang et al. [5, 6] and Choubey et al. [7, 8] made a detailed overview of the research work of the transverse jet in the supersonic flow. At present, the investigation on mixing enhancement approaches is mainly to explore new mixing enhancement devices or capture the fine structure of the flow field through higher precision numerical approaches.

Applying unsteady excitation to the jet is a novel hybrid enhancement approach. Randolph et al. [9] first used the wind tunnel to study the pulsed jet in a supersonic flow. In this study, the pressure at the outlet of the pulsed jet is always in the steady state. The obtained results show that the jet penetration depth can be improved without increasing the momentum flux ratio. After comparing different oscillation laws, Narayan et al. [10] found that when the exciting jet changes in a sinusoidal law, it can increase the penetration depth to the maximum and greatly improve the mixing effect.

It is found that the pulsed frequency between 10 and 50kHz is the effective frequency that affect the mixing process, and the jet frequency outside this range will cause a penetration effect similar to that of the steady jet [11]. Kouchi et al. [12] suggested that in order to better compare the effects of the pulsed and steady jets, the average mass flow of the pulsed jet in a cycle should be consistent with that of the steady jet. Later, they [13] studied the impact of the pulsed jet in combination with the ground experimental tests and numerical approaches. The obtained results show that compared with the steady jet flow field, 10–20kHz pulsed jet can effectively improve the penetration depth. When the frequency is close to 50kHz, the pulsed jet shows the same behaviour as the steady jet, and this is basically consistent with the obtained results of Cutler et al. [11] However, the flexibility of the best frequency for the pulsed jet has not been explored, and it should be solved by means of the multi-objective design optimisation approaches.

Shi et al. [14] used the large eddy simulation approach to study the transverse pulsed jet flow field in a supersonic crossflow, and the numerical simulation captured the complex flow field structures. The work of Williams et al. [15] shows that within a certain frequency range, the pulsed jet can improve the jet penetration depth and mixing efficiency without increasing total pressure loss. Li et al. [16] studied the influence of the pulsed jet flow field structure and mixing effect by placing a small ramp of delta wing upstream of the injector and applying pulse to jet. The results show that the mixing efficiency of the steady flow field with low jet-to-crossflow pressure ratio is better than that of excited jet flow field. When the jet-to-crossflow pressure ratio increases, the mixing efficiency of excited jet flow field begins to be higher than that of the steady jet flow field. Therefore, when the jet-to-crossflow pressure ratio is taken within a certain range, the excited jet flow field is better than the steady jet flow field. Du et al. [17] applied the pulsed jet to the fuel injection of the shock induced ramjet forebody/inlet. It is found that the intermittent injection of the pulsed jet has unique advantages in reducing the total pressure loss and improving the fuel penetration depth. The role of the pulsed jet is more obvious at higher jet-to-crossflow pressure ratio.

Zhao et al. [18] studied the flow field of the hydrogen pulsed jet under high enthalpy inflow by using OpenFOAM. According to the predicted results, the flow state is studied, and the pulsed frequency with better mixing efficiency and penetration depth is 50kHz, improving with the increase of the pulsed amplitude. The variation of the pulsed frequency and amplitude does not cause the variation of the total pressure loss. After that, it uses the wavelet analysis to connect the pulsed frequency with the characteristic frequency of the flow field structure, and a better frequency of 40kHz is obtained at last [19].
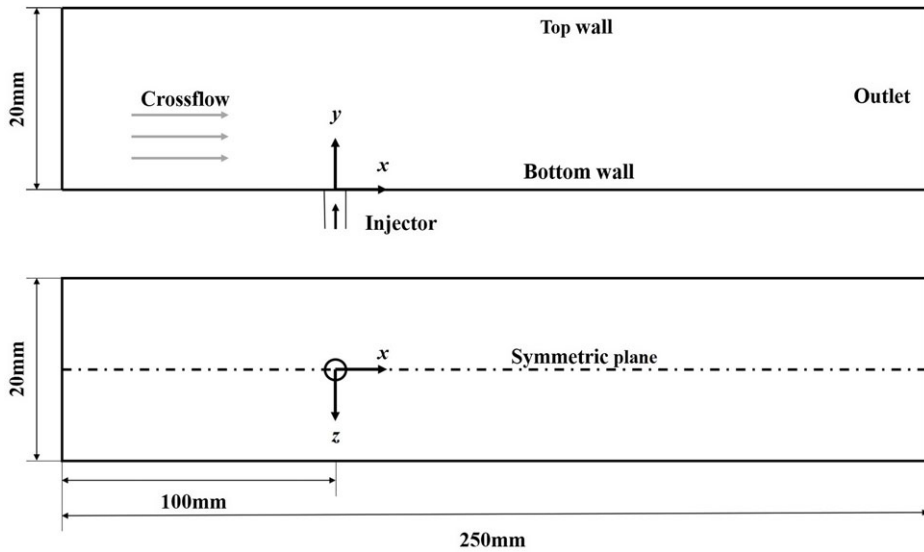
Figure 1. *Schematic diagram of the physical model employed in the current study.*

From the above analysis, it is observed that there are relatively few studies on the pulsed jet at present, and consistent understanding of its mixing enhancement mechanism has not been obtained, especially for its best frequency on the mixing augmentation process. It may change with the variation of the boundary conditions, as well as the specific configuration employed. In order to explore the impact of the pulsed frequency on the jet flow field structures and mixing effect in a real scramjet engine tested in our laboratory, the three-dimensional RANS approaches are employed, selecting the pulsed excitation with different frequencies, and comparing them with its corresponding steady flow field to explore the influence of the pulsed frequency on the performance of the jet flow field. This is an important step for its surrogate model setting and optimisation in the next step. Section 2 introduces the physical model and numerical method, Section 3 analyses the impact of the pulsed frequency on the jet flow field, and the last section provides some conclusions for this study.

2.0 Physical model and numerical method

2.1 Physical model and flow parameters

The physical model is a rectangular channel, which is 250mm long, 20mm wide and 20mm high, and these values are chosen in order to consider the wall effect on the working process in a real scramjet engine for its engineering application. An injector with its diameter being 2mm is set on the bottom wall of the channel. The geometric structure of the calculation domain is shown in Fig. 1. The incoming flow is from left to right. The coordinate origin is set at the centre of the injector, and it is 100mm away from the inlet of the incoming flow. The whole flow field is symmetrical about the XOY plane.

The flow parameters are consistent with the work of Erdem et al. [20] The incoming flow is air, and it is composed of 21% oxygen and 79% nitrogen. The jet is hydrogen, with its jet angle being 90°, and the jet momentum flux ratio (J) is 1.85. The jet momentum flux ratio is defined as the ratio between the momentum fluxes on the jet exit and in the crossflow, and its equation can refer to Ref. [5]. Table 1 shows the specific flow parameters of the incoming flow and the jet. Due to the symmetry of the flow field, half of the calculation domain is selected for this solution. The boundary conditions are set as follows, namely the supersonic incoming flow is set as the far pressure field, the fuel injector is set as the pressure inlet, the downstream outlet boundary is the pressure outlet, and the other surfaces are no slip wall.

The waveform of the pulsed jet is sine wave, and the frequencies are $f_1 = 12.5$kHz, $f_2 = 20$kHz and $f_3 = 50$kHz, respectively. The pulsed realisation of the jet outlet relies on the user-defined function (UDF), and it shows the change law of the pulsed jet with the variation of the momentum flux ratio.

$$J = J_0 + J_a \times \sin(2 \times 3.14159\, ft) \tag{1}$$

Herein, J is the momentum flux ratio which varies with time, and J_0 is the benchmark momentum flux ratio. J_a is the amplitude of sinusoidal variation, and its value is 1.0. f is the frequency of sine wave, and t is the flow time in the flow field.

In order to make the calculation results of the pulsed jet stable and reliable, the calculation of the unsteady flow field is started on the basis of the steady state of the basic calculation example, and the UDF is loaded by compiling. In the process of calculating each time step, when the residual curve drops by more than three orders of magnitude and remains stable, it is considered that the time step converges. In the unsteady state calculation, the time steps of f_1, f_2 and f_3 frequency pulsed jets are set to be 4.0×10^{-6}s, 2.5×10^{-6}s and 1.0×10^{-6}s, respectively.

2.2 Numerical approach and validation

The structured grids of the computational domain are obtained by the ANSYS ICEM, and the numerical simulation is conducted by means of the ANSYS Fluent. Then, Tecplot and Origin are used for post-processing of computational results. At the same time, a parallel computing environment provided by Beijing Supercomputing Center is utilised to improve the computational efficiency. The flow field is solved based on the cell centred finite volume method, and the SST·k-ω model is selected as the turbulence model. An implicit, steady/unsteady solver based on density coupling is used to solve the three-dimensional compressible Reynolds-averaged Navier Stokes (RANS) equations. The upwind scheme with spatial second-order accuracy, AUSM vector splitting scheme and green Gauss·cell-based gradient calculation method are utilised, and the CFL number is keep as 0.5 during the calculation process.

The RANS method solves the averaged control equations. After Favre averaging, the transport equations can be obtained. In order to verify the calculation accuracy of the numerical method adopted in this paper, a numerical simulation is conducted based on the ground experiment of a transverse jet in the supersonic crossflow conducted by Santiago et al., [21] and the calculation results are compared with the available test data captured from the experimental velocity contours which are also available in Ref. [22]. In this test, the materials for the crossflow and transverse jet are both set to be air, and the ratio of its specific heat is 1.4. Three mean velocity components were measured through the two-component, frequency preshifted laser Doppler velocimetry. The Mach number of the crossflow is 1.6, with its static pressure and temperature being 56.7kPa and 198K, respectively. For the jet, the Mach number is 1.0, the static pressure is 247KPa, and the static temperature is 250K. The momentum flux ratio is 1.7. The calculation domain is a rectangular channel, with its dimensions being $-37.5 < x/D < 37.5$, $0 < y/D < 9$, $-9.5 < z/D < 9.5$. Herein, D is the diameter of the injector, with its value being 4mm, and the coordinate origin is set at the centre of the injector.

In order to ensure that y^+ is less than 1.0, the height of the first layer of grid on the wall is set to be 0.001mm, and the elements are refined in the area with complex flow fields near the injector. In order to ensure the reliability of the calculation results and avoid the influence of mesh size, three mesh sizes are selected for calculation, and the mesh independence is verified. The number of elements are 2.0 million, 2.5 million and 3.0 million, respectively. Figure 2 shows the division results of the moderate grid employed in the current study.

Figure 3 shows the calculation results of three mesh sizes, which respectively represent the distribution of dimensionless flow velocity along the normal direction at different flow positions ($x/D = 4, 5$) which are on the centre of the symmetry plane. The obtained results show that the mesh size only has little effect on the calculation results, and there is little difference between the moderate and fine meshes

Table 1. *Flow parameters employed in the current study*

	Mach number	Static pressure (Pa)	Static temperature (K)
Crossflow	2.6	6,709	135.2
Jet	1.0	83,998	248.3
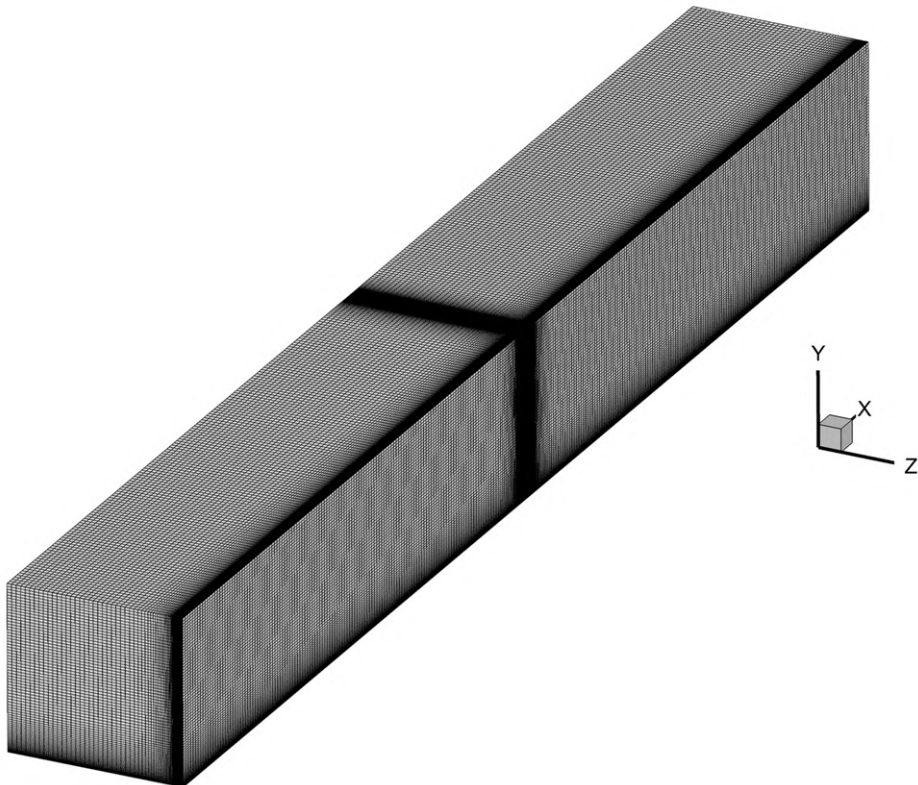
Figure 2. *Schematic diagram of the moderate grid employed in the current study.*

mostly. The numerical method can effectively obtain the characteristics of the flow field, and the predicted results are in good agreement with the available experimental data in terms of trend and value. This may imply that the numerical method is reliable for subsequent calculations.

3.0 Calculation results and discussion

3.1 Time evolution characteristics of flow field

In order to analyse the change law of the pulsed jet flow field structure in a cycle, the pulsed jet flow field with a frequency of 50kHz is selected to show the flow field structure at different times in a cycle.

Figure 4 shows the contours of hydrogen mole fraction on the central symmetry plane at different times. 0/4T represents the starting point of upward movement in this cycle. At this time, the instantaneous jet momentum flux ratio of the pulsed jet is 1.85, and this is the same as the steady jet. The main effect of the pulsed jet on the flow field is form a high-low alternating wavy structure in the flow field. The appearance of this structure makes the hydrogen surface in the flow field no longer smooth. At the wavy structure, there is a high hydrogen concentration, and the wavy structure appears intermittently in the flow direction, which has an important impact on the mixing performance of the fuel jet.
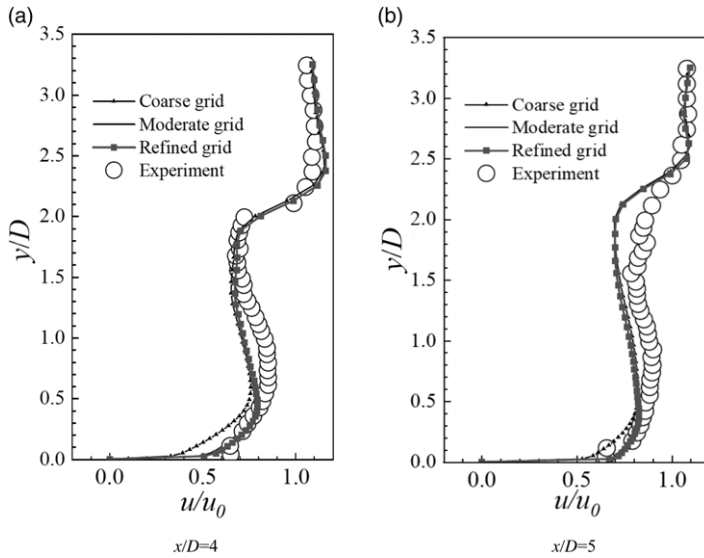
Figure 3. *Comparison of numerical and experimental nondimensional velocities in the flow direction.*
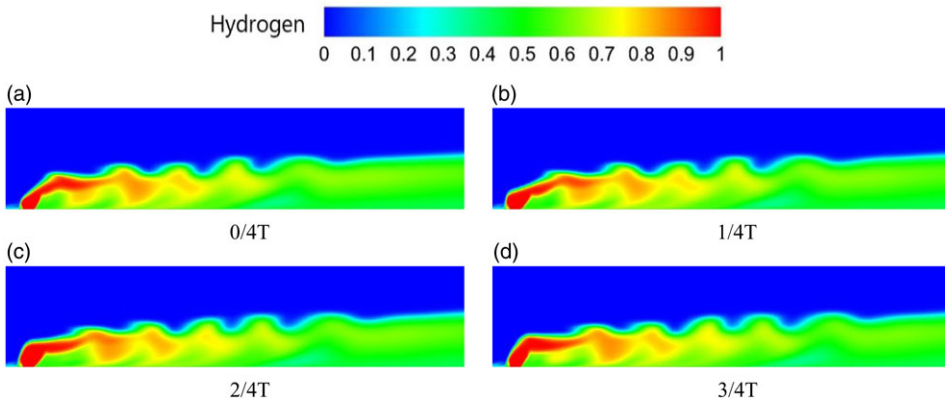

Figure 4. *Hydrogen mole fraction contours on the symmetry plane at different times.*

The shape of the hydrogen core near the injector is different at different times. At 0/4T, the area of the hydrogen core is the smallest, and its tilt angle is the largest. At 1/4T and 2/4T, the hydrogen cores are larger in the flow field, their flow fields are more similar, and the differences in the hydrogen core and the structures of the recirculation region are smaller. The flow field structure at 3/4T is similar to that at 0/4T.

The flow positions of the jet downstream wavy structure are different at different times. The wavy structure will move downstream of the jet with time. In the early stage of the formation of the wavy structure, the hydrogen surface near the injector will form a bulge, where the jet penetration depth will be improved, which is conducive to the normal transportation of fuel, generating a larger normal distribution, and avoiding the accumulation of heat on the wall during combustion. With the development of time, the wavy structure will be separated from the mainstream of the jet in the influence of the crossflow, and forming an independent structure. The flow distance of the wavy structure in the flow field is about 10mm, and almost only one structure is formed in a cycle. Therefore, it takes some time for the pulsed jet to establish its influence in the whole flow field.
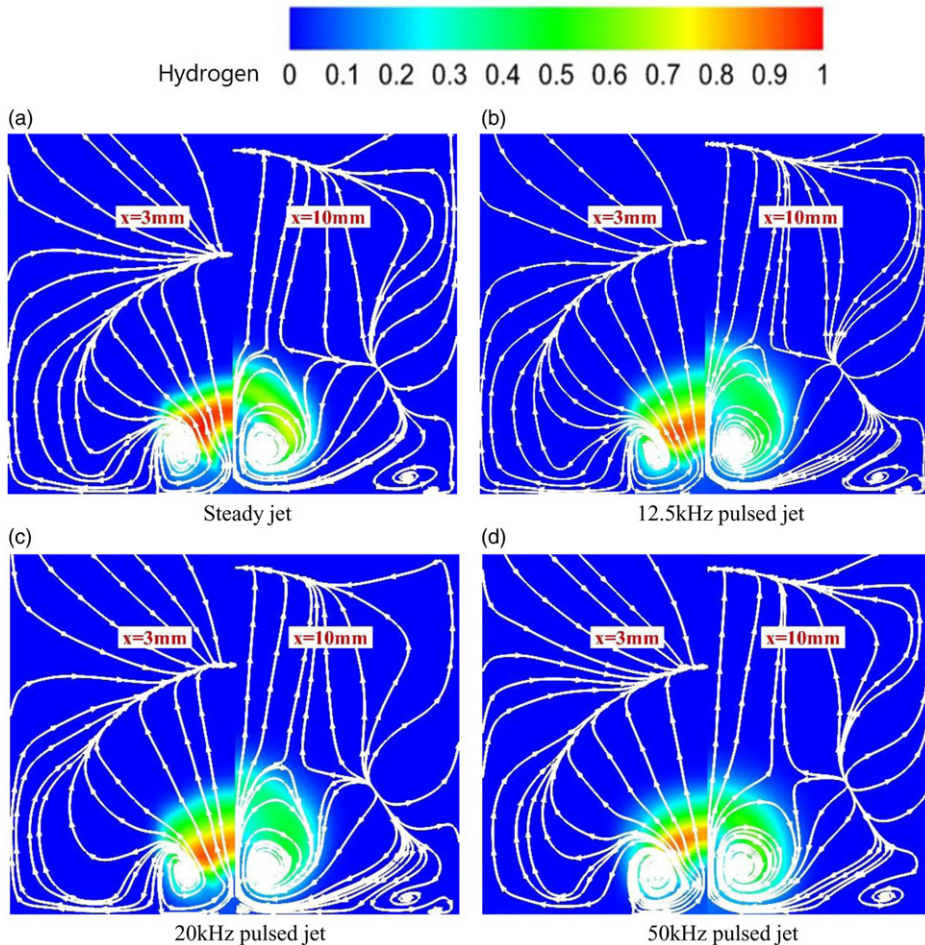
Figure 5. *Hydrogen mass fraction contours and streamlines on cross-sectional planes located at x = 3mm and 10 mm of steady jet and the mean flow field of pulsed jet.*

3.2 Comparative analysis of steady jet flow field and pulsed mean flow field

In this section, the steady jet flow field and the mean flow field of the pulsed jet are compared and analysed. The mean flow field is the average of two cycles of flow after the pulsed effect is established in the whole flow field.

Figure 5 shows the steady jet and the mean flow field structures of three different frequencies. The contours of hydrogen mass fraction and streamlines are shown on the $x = 3$ and 10mm cross-sectional planes. According to the hydrogen mass fraction contours in Fig. 5, the hydrogen concentration in the $x = 3$ and 10mm cross-sectional planes of the steady jet is greater than that in the mean flow field of the pulsed jet, indicating that the mixing efficiency of the pulsed jet is higher, and the mixing is complete earlier for the pulsed jet. Among them, the hydrogen concentration are the smallest on the 50kHz jet, and this means that the mixing efficiency are the highest for these conditions employed in this study. The hydrogen distributions of the two low-frequency pulsed jets on the $x = 10$mm cross-sectional plane are higher in the normal direction, and they have the highest penetration at this time. However, in the 50kHz jet, the fuel distribution shown in Fig. 5 almost have not raised in the normal direction.

In order to analyse the mixing in the transverse jet flow field, the mixing efficiency, the total pressure recovery coefficient and jet penetration depth are all selected for analysis.

Table 2. *Boundary condition settings for different cases*

	Pulse frequency (kHz)	The momentum flux ratio
Case1	0	1.85
Case2	12.5	1.85
Case3	20	1.85
Case4	50	1.85

The mixing efficiency is used to evaluate the mixing and combustion process along the flow direction. It is defined as the ratio of the fuel mass flow passing the flow cross-sectional planes that can participate in the combustion to the total fuel mass flow. Its expression is shown in the formula (2) [23].

$$\eta_{mix}(x) = \frac{\int_A \alpha_{react} \rho u dA}{\int_A \alpha \rho u dA} \tag{2}$$

$$\alpha_{react} = \begin{cases} \alpha & \alpha \leq \alpha_{stoic} \\ \alpha_{stoic}(1-\alpha)/(1-\alpha_{stoic}) & \alpha > \alpha_{stoic} \end{cases} \tag{3}$$

The fuel is hydrogen, ρ is the local density, u is the local velocity, A is the axial area of mixing, α is the mass fraction of fuel, α_{stoic} is the mass fraction of fuel at the chemical equivalence ratio. For hydrogen, this value is 0.0283. From the expression, when the mass fraction of hydrogen is less than 0.0283, hydrogen and air are mixed, and the mixing efficiency reaches 1.0.

The penetration depth is an important characteristic parameter of the engine. It is calculated according to the fuel centroid, and its expression is shown in the formula (4) [24].

$$P_{H_2}(x) = \frac{\int_A \alpha \rho u y dA}{\int_A \alpha \rho u dA} \tag{4}$$

The total pressure recovery coefficient is the ratio of the local total pressure to the crossflow total pressure, and it can reflect the thrust of the engine.

Figure 6 shows the mixing efficiency, penetration depth and total pressure recovery coefficient curves of steady and pulsed jets. From the mixing efficiency curve, the application of the pulsed jet can enhance the mixing effect of flow field. Among them, the mixing efficiency of 50kHz pulsed jet is higher, the influence of two low-frequency pulsed jet on the mixing of flow field is mainly reflected in the far-field downstream of the jet, and the mixing efficiency is significantly improved in the far-field. In the penetration depth curve, the 50kHz pulsed jet can improve the penetration depth of the downstream far-field region. In the near field, the penetration depth of the low-frequency pulsed jet is deeper. However, in the downstream of the flow field, the penetration depth will first decrease and then increase, and the penetration depth of the steady jet is above them finally. The pulsed jet has little effect on the total pressure recovery coefficient at the outlet of the channel.

3.3 Comparative analysis of steady jet and pulsed instantaneous flow field

In this section, the steady jet reference case and the instantaneous flow field structure of the pulsed jet will be analysed. The instantaneous jet momentum flux ratio of the pulsed jet is 1.85, and it is in the upward range of the sine wave. For the convenience of subsequent analysis, different cases are named as Case1–Case4, and their boundary condition settings are shown in Table 2.

Figure 7 shows the contours of hydrogen mass fraction on the cross-sectional planes of $x = 0$, 5, 10, 15, 20 and 25mm, and the red solid line represents the streamline of hydrogen mass fraction being 0.01, which can represent the normal and spanwise hydrogen distribution on the section.

Figure 7(a) represents the case of the steady jet. The hydrogen has just left the injector and gathered in a relatively concentrated area. In the process of flowing downstream, it is gradually divided into two parts, and there is an obvious gap between the hydrogen plumes in the two parts.
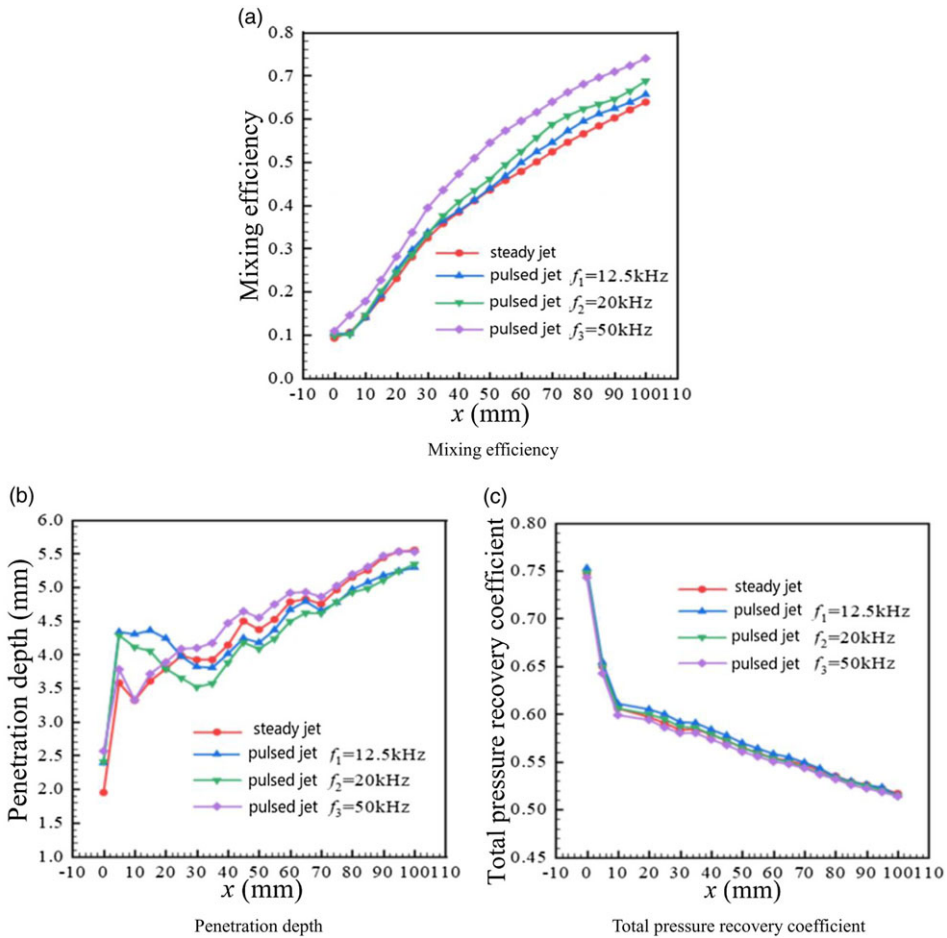
Figure 6. *Comparison of mixing parameters of steady jet and the mean flow field of pulsed jet.*

In the process of hydrogen flowing downstream in the pulsed jet, the region with high hydrogen concentration will appear intermittently, and this indicates that the pulsed impact on the jet flow field exists. On the cross-sectional plane of $x = 0$mm, the steady jet plume occupies a larger area, while the plumes of the three unsteady flow fields are relatively concentrated in a smaller area. At this time, the steady flow field has deeper normal penetration and spanwise distribution at the jet outlet. On the $x = 5$mm cross-sectional plane, Case1 has the highest hydrogen concentration, Case4 has the lowest hydrogen concentration and the core of the plume is at a higher position. The hydrogen distributions of Case2 and Case3 are basically similar except for different distributions in the spanwise width. Therefore, at this position, the steady jet has a lower mixing efficiency, the pulsed jet of 50kHz has a higher mixing efficiency, and the two pulsed jets with relatively low frequency have the same mixing efficiency. Moreover, the hydrogen at 50kHz has higher penetration depth and spanwise distribution.

In the process of flowing downstream, Case4 first appears the first high concentration area of hydrogen, which is at the position of $x = 20$mm. The mixing between the hydrogen and the crossflow is greatly affected here, the mixing effect here decreases significantly when compared with its previous cross-sectional planes, the hydrogen plumes on this cross-sectional plane gather again, and the previous gap no longer exists. However, the high concentration area of hydrogen in Case3 appears at a later position than Case4, where $x = 25$mm, and its concentration has increased more than Case4. The hydrogen mixing becomes worse here, it can be seen that Case3 has a lower mixing efficiency here. The hydrogen
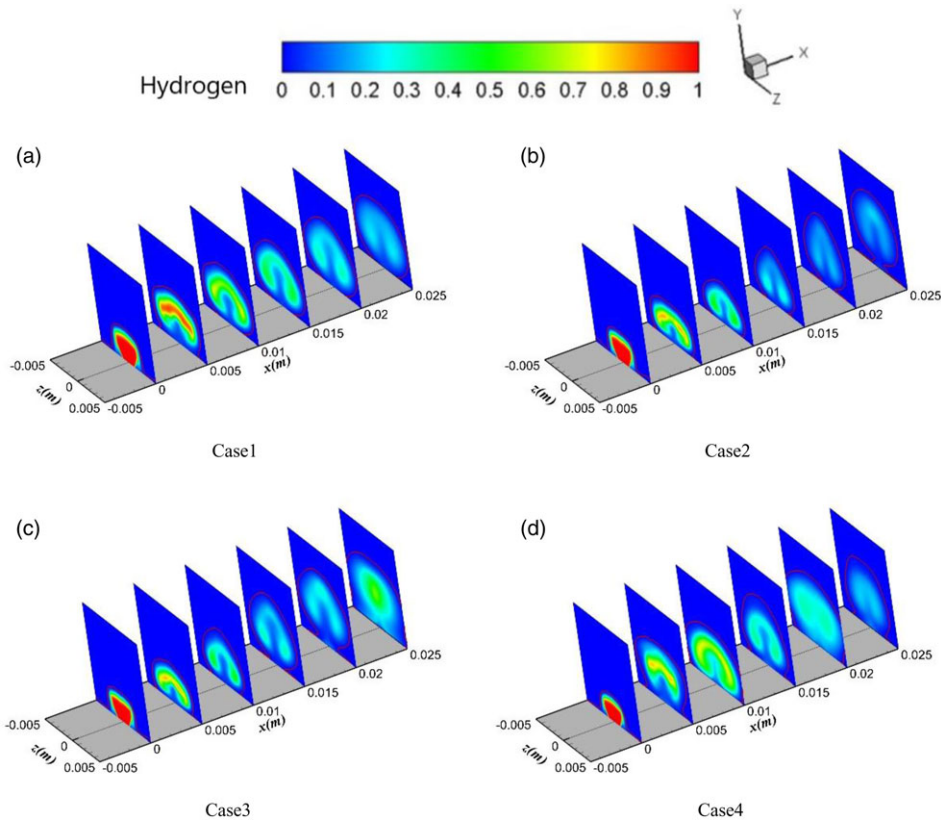
Figure 7. *Hydrogen mass fraction contours and 0.01 streamline on the cross-sectional planes.*

concentration of Case2 at $x = 15$, 20 and 25mm is the lowest. At this time, its mixing is more efficient. On the cross-sectional plane shown in Fig. 7, Case2 has not yet appeared the first high hydrogen concentration area, and it should be in a more backward position.

Figure 8 shows the contours and streamlines of hydrogen mole fraction on the cross-sectional planes of $x = 5$ and 20mm. On the $x = 5$mm cross-sectional plane, the counter rotating vortex pair is basically under the hydrogen plume, while on the $x = 20$mm cross-sectional plane, the position of the core of counter rotating vortex pair is basically equivalent to the core of plume, indicating that the vortex structure plays an important role in the fuel transportation process, in the process of flowing downstream, the size of the vortex pair will increase, and the greater the role of the vortex pair on fuel transportation. The area occupied by the hydrogen plume of Case4 on the section of $x = 5$mm is the largest, and its concentration is also the lowest, the frequency of 50kHz on this section has the highest mixing efficiency and deepest penetration depth, which is consistent with the above conclusion. Case2 and Case3 are affected by the pulse, the areas occupied by the hydrogen plume decrease, and the hydrogen penetration reduces, but their mixing efficiencies improve that of the steady state. In the two low-frequency jet, the wake vortex structure appears on the section $x = 5$mm, but does not appear in the other two frequencies. On the $x = 25$mm section, Case1 and Case4 have a similar jet penetration depth, but Case4 has a higher mixing efficiency, and its penetration depth is weaker than that of the $x = 5$mm section, while the penetration depth in Case1 is improved, and the hydrogen spanwise width of Case4 is also less than that of Case1.

Figure 9 shows the contours and streamlines of hydrogen mole fraction on the central symmetry plane, in which the structure of the two upstream reflux areas and the downstream low-speed reflux area can be observed.
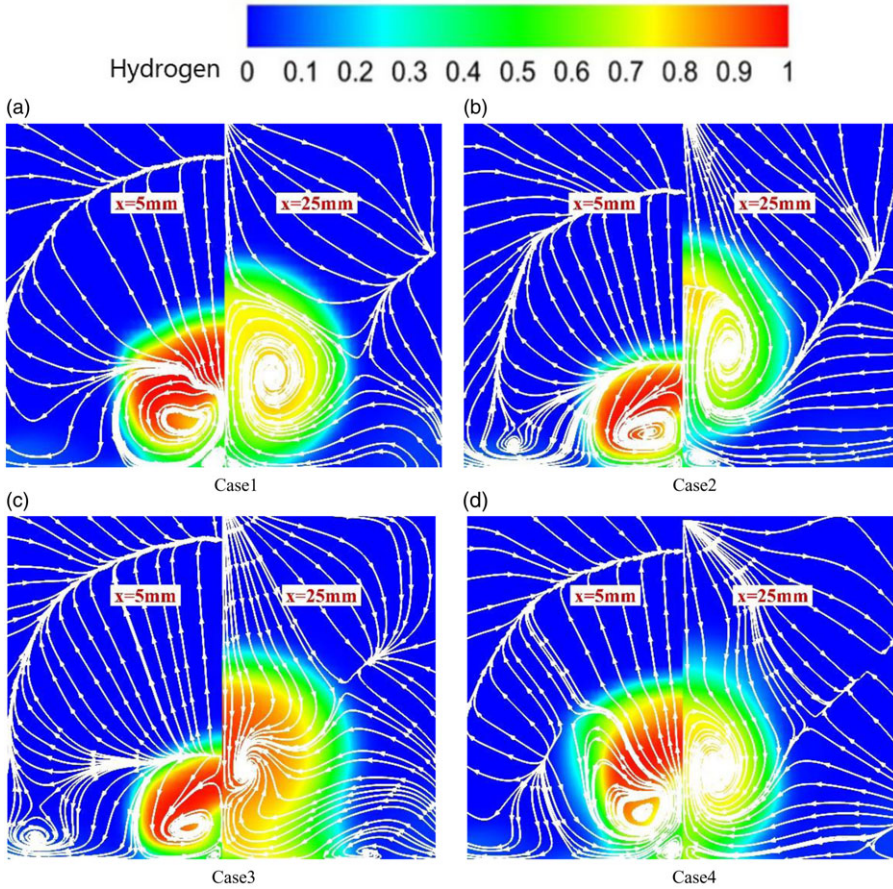
Figure 8. *Hydrogen mole fraction contours and streamlines on the cross-sectional planes located at x = 5mm and 25mm.*
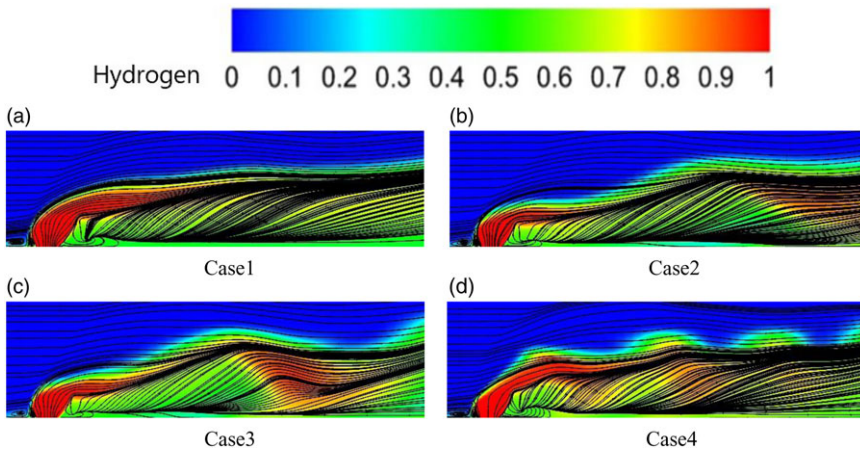

Figure 9. *Hydrogen mole fraction counters and streamlines on the symmetric plane.*
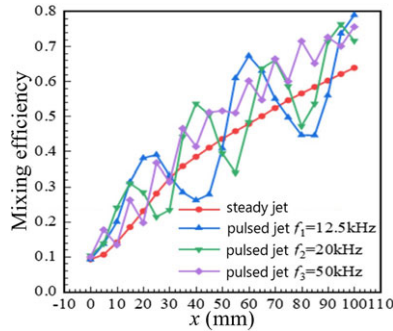
Figure 10. *Comparison of mixing efficiencies between steady and pulsed jets with different frequencies.*

It can be seen from Fig. 9(a) that in the steady jet, the surface of the hydrogen core is relatively smooth, the concentration of hydrogen decreases along the flow direction, and the penetration depth increases. Compared with Fig. 9(a)–(d), the pulsed jet increases the unsteady characteristics of the flow field. Under the action of the pulse, the surface of the hydrogen plume twists and turns, and the uneven wavy structure appears. The hydrogen distribution of Case2 and Case3, the two low-frequency pulse, is relatively similar, and the main difference is in the positions of the first hydrogen high concentration area in the downstream and the size of the upstream reflux area. In Case2, the location of the downstream high concentration area is relatively backward, and the low concentration area downstream of the jet occupies a larger area, which is also the reason why the high concentration area is not shown in Fig. 7(b). In Case3, the appearance of this area is earlier, and the appearance of this high concentration area represents that the fuel mixing is not completed well. It is found that the increase of pulses frequency reduces the downstream low concentration area occupy.

In Fig. 9(d), the pulsed frequency is 50kHz, which causes the wavy structure on the surface of hydrogen in the flow field to show intensive, the distance between the wavy structure is small, and hydrogen is mainly distributed in the near-field area downstream of the jet. Compared with the flow field of low pulsed frequency, the pulsed frequency of the hydrogen jet is faster, but the amplitude of the fluctuation is not as large as that of the low-frequency pulsed jet flow field, the spanwise area of the hydrogen in the downstream near-field area on the wall is larger and gradually decreases along the flow direction, which is different from the development law of the wall hydrogen distribution of the low-frequency jet.

Figure 10 shows the mixing efficiency curves of steady jet and pulsed jets. In the unsteady jet flow field, the high concentration region of hydrogen mass will appear intermittently downstream, which will cause the repeated process of the mixing efficiency enhanced-weakened-enhanced in the flow field. Compared with Case3, the turning point of the curve in Case2 lags behind, while Case4 has a relatively short distance of the wavy structure in the flow field, and through the fluctuation of its mixing efficiency curve, it is obviously different from the low-frequency jet cases.

The mixing efficiency of Case4 basically fluctuates above the steady jet curve, that is, the 50kHz pulsed jet has high mixing efficiency in the whole region. Pulsed jet can enhance the mixing of transverse jet flow field, 50kHz pulsed jet can improve the mixing efficiency almost the whole flow field, while low-frequency pulsed jet will cause great fluctuation of mixing efficiency in the flow field, which may be detrimental to the working process of the engine.

According to the expression of jet penetration depth, the penetration depths on different flow cross-sectional planes are calculated and drawn into Fig. 11. In the near-field region, Case4 has advantages over other cases in improving the penetration depth of the jet, but after the pulsation of Case2 and Case3 begin, Case4 loses this advantage. Downstream of the jet, the penetration depth of all pulsed jet cases begins to fluctuate around the steady curve.
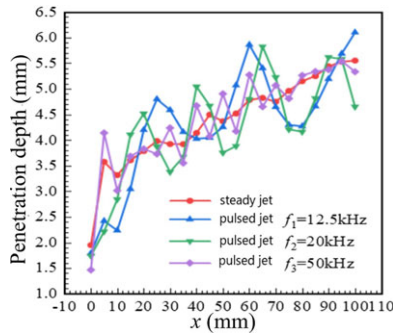
Figure 11. *Comparison of penetration depths between steady and pulsed jets with different frequencies.*

4.0 Conclusions

The three-dimensional conservation equations are solved by means of the Reynolds-averaged Navier–Stokes (RANS) approaches combined with the SST k-ω turbulence model, and the influence of pulsed jet with different frequencies ($f_1 = 12.5\text{kHz}$, $f_2 = 20\text{kHz}$ and $f_3 = 50\text{kHz}$) on the mixing effect of fuel and air in a supersonic crossflow is studied. The flow field structures and mixing effect of pulsed jet at different times in a cycle are analysed, and the following conclusions have been drawn.

(1) The action of the pulsed jet will change the instantaneous structure of the flow field and produce a wavy structure in the flow field, and the flow field structures of the pulsed jet are different at different times in a cycle. The wavy structure generated in the flow field will move downstream of the flow field with time, and it takes a certain time for the pulsed jet to establish its influence in the full flow field.

(2) In the comparison of steady flow field and pulsed mean flow field, it is found that pulsed jet can improve the mixing efficiency of flow field. Among them, the mixing efficiency of pulsed jet with frequency of 50kHz is better in the three frequencies employed in the current study, and the penetration depth in the downstream is larger, and the effect of pulsed jet has little effect on the variation of the total pressure recovery efficient.

(3) In the action of 12.5 and 20kHz pulsed frequencies, the overall structures of the flow field are relatively similar, and there will be an intermittent high concentration area of hydrogen downstream of the jet, resulting in the reduction of mixing efficiency. However, the locations of the first occurrence of this area in the two cases are different, which may be related to the pulsed frequency. However, under the 50kHz jet frequency, the wavy structure in the flow field is relatively compact, which can enhance mixing.

Conflict of interest. The authors declare there is no conflict of interest regarding the publication of this paper.

Data availability. The data that supports the findings of this study are available within this paper.

References

[1] Huang, W., Liu, J., Jin, L. and Yan, L. Molecular weight and injector configuration effects on the transverse injection flow field properties in supersonic flows, *Aerosp Sci Technol*, 2014, **32**, (1), pp 94–102.

[2] Lee, S.H. Characteristics of dual transverse injection in scramjet combustor, part 2: Combustion, *J Propul Power*, 2006, **22**, (5), pp 1020–1026.

[3] Sun, M.B. and Hu, Z.W. Formation of surface trailing counter-rotating vortex pairs downstream of a sonic jet in a supersonic cross-flow, *J Fluid Mech*, 2018, **850**, pp 551–583.

[4] Watanabe, J., Kouchi, T., Takita, K. and Masuya, G. Large-eddy simulation of jet in supersonic crossflow with different injectant species, *AIAA J*, 2013, **50**, (12), pp 2765–2778.

[5] Huang, W. Transverse jet in supersonic crossflows, *Aerosp Sci Technol*, 2016, **50**, pp 183–195.

[6] Huang, W. Mixing enhancement strategies and their mechanisms in supersonic flows: A brief review, *Acta Astronaut*, 2018, **145**, pp 492–500.

[7] Choubey, G., Yuvarajan, D., Huang, W., Yan, L., Babazadeh, H. and Pandey, K.M. Hydrogen fuel in scramjet engines - A brief review, *Int J Hydrogen Energy*, 2020, **45**, (33), pp 16799–16815.

[8] Choubey, G., Yuvarajan, D., Huang, W., Shafee, A. and Pandey, K.M. Recent research progress on transverse injection technique for scramjet applications-a brief review, *Int J Hydrogen Energy*, 2020, **45**, (51), pp 27806–27827.

[9] Randolph, H., Chew, L. and Johari, H. Pulsed jets in supersonic crossflow, *J Propul Power*, 1994, **10**, pp 746–748.

[10] Narayanan, S., Barooah, P. and Cohen, JM. Dynamics and control of an isolated jet in crossflow, *AIAA J*, 2003, **41**, (12), pp 2316–2330.

[11] Cutler, A., Harding, G. and Diskin, G. High frequency supersonic pulsed injection, 39th Aerospace Sciences Meeting and Exhibit, 2001.

[12] Kouchi, T., Sakuranaka, N., Izumikawa, M. and Tomioka, S. Pulsed transverse injection applied to a supersonic flow, 43rd AIAA/ASME/SAE/ASEE Joint Propulsion Conference & Exhibit, 2007.

[13] Kouchi, T., Sasaya, K., Watanabe, J., Shibayama, H. and Masuya, G. Penetration characteristics of pulsed injection into supersonic crossflow, 46th AIAA/ASME/SAE/ASEE Joint Propulsion Conference & Exhibit, 2010.

[14] Shi, H.T., Wang, G.L., Luo, X.S., Yang, J.M. and Lu, X.Y. Large-eddy simulation of a pulsed jet into a supersonic crossflow. *Comput Fluids*, 2016, **140**, pp 320–333.

[15] Williams, N.J., Moeller, T.M. and Thompson, R.J. Numerical simulations of high frequency transverse pulsed jet injection into a supersonic crossflow, *Aerosp Sci Technol*, 2020, **103**, p 105908.

[16] Li, L.Q., Huang, W., Yan, L., Zhao, Z.T. and Liao, L. Mixing enhancement and penetration improvement induced by pulsed gaseous jet and a vortex generator in supersonic flows, *Int J Hydrogen Energy*, 2017, **42**, (30), pp 19318–19330.

[17] Du, Z.B., Huang, W., Yan, L. and Li, S.B. Reynolds-average Navier-Stokes study of steady and pulsed gaseous jets with different periods for the shock-induced combustion ramjet engine, *Phys Fluids*, 2019, **31**, (5), p 055107.

[18] Zhao, M.J. and Ye, T.H. URANS study of pulsed hydrogen jet characteristics and mixing enhancement in supersonic crossflow. *Int J Hydrogen Energy*, 2019, **44**, (36), pp 20493–20503.

[19] Zhao, M.J., Li, Q.L. and Ye, T.H. Investigation of an optimal pulsed jet mixing and combustion in supersonic crossflow, *Combust Flame*, 2021, **227**, pp 186–201.

[20] Erdem, E. and Kontis, K. Numerical and experimental investigation of transverse injection flows, *Shock Waves*, 2010, **20**, (2), pp 103–118.

[21] Santiago, J.G. and Dutton, J.C. Velocity Measurements of a Jet Injected into a Supersonic Crossflow. *J Propul Power*, 1997, **13**: 264–273.

[22] Kawai, S. and Lele, S.K. Large-eddy simulation of jet mixing in supersonic crossflows. *AIAA J*, 2010, **48**, (9), 2063–2083.

[23] Gerlinger, P., Stoll, P., Kindler, M., Schneider, F. and Aigner, M. Numerical investigation of mixing and combustion enhancement in supersonic combustors by strut induced streamwise vorticity, *Aerosp Sci Technol*, 2008, **12**, (2), pp 159–168.

[24] Lee, S.H. and Mitani, T. Mixing augmentation of transverse injection in scramjet combustor. *J Propul Power*, 2003, **19**, (1), pp 115–124.